RIGA TECHNICAL UNIVERSITY

Māris Rundāns

POROUS CORDIERITE CERAMICS FROM MINERAL AND SYNTHETIC RAW MATERIAL COMPOSITIONS

Summary of the Doctoral Thesis

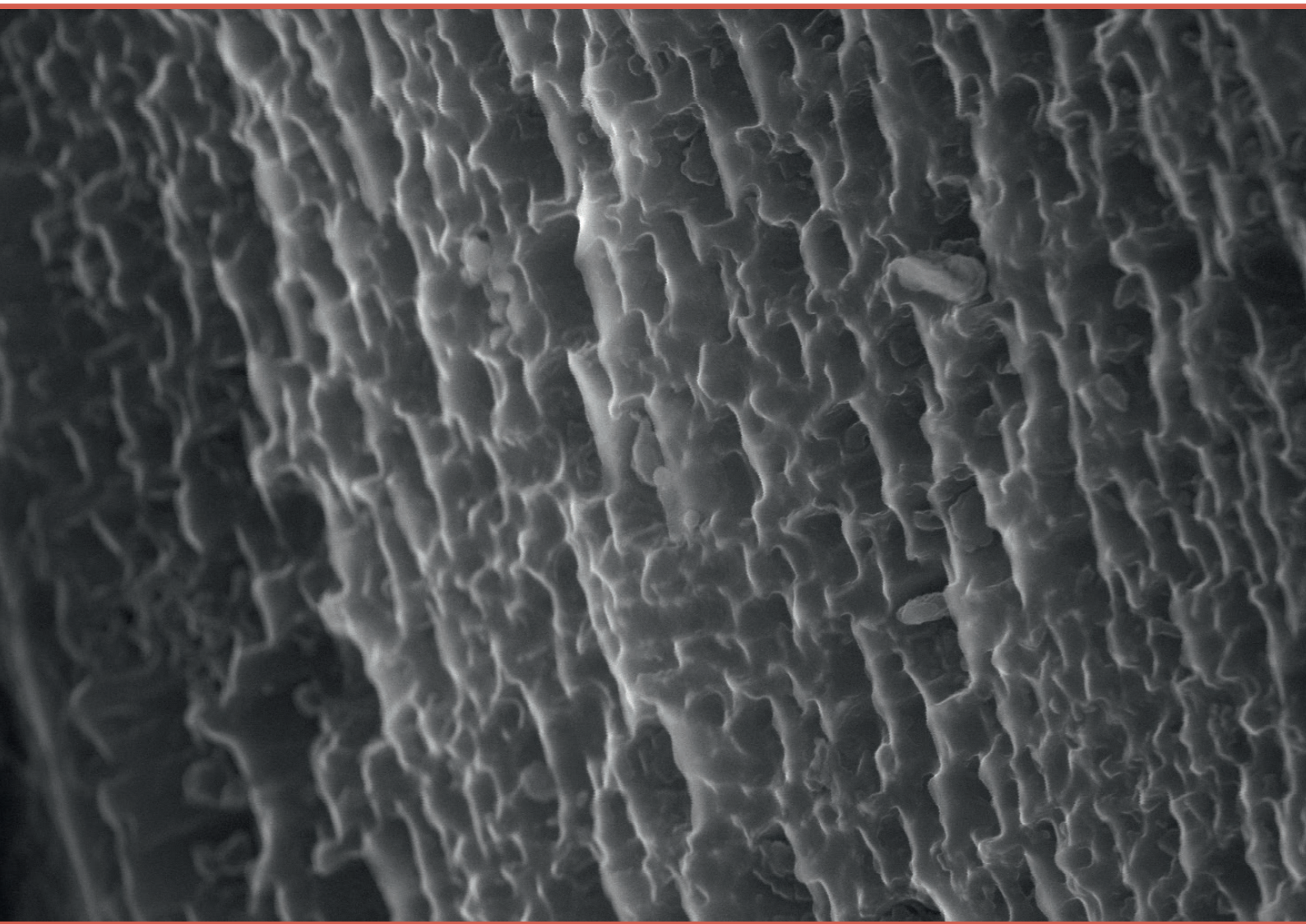

RTU Press
Riga 2021

RIGA TECHNICAL UNIVERSITY
Faculty of Materials Science and Applied Chemistry
Institute of Silicate Materials

Māris Rundāns
Doctoral Student of the Study Programme "Chemical Technology"

POROUS CORDIERITE CERAMICS FROM MINERAL AND SYNTHETIC RAW MATERIAL COMPOSITIONS

Summary of the Doctoral Thesis

Scientific supervisor
Dr. habil. chem.
GAIDA MARUTA SEDMALE

RTU Press
Riga 2021

Rundāns, M. Porous Cordierite Ceramics From Mineral and Synthetic Raw Material Compositions. Summary of the Doctoral Thesis. Riga: RTU Press, 2021. 37 p.

Published in accordance with the decision of the Promotion Council "RTU P-01" of 18 September, 2020, Minutes No. 04030-9.1/9.

Acknowledgement

I would like to express my deepest gratitude to my supervisor, Dr.habil.chem. Gaida Maruta Sedmale for the invaluable help and advice provided during the development of the dissertation.

I would also like to thank my colleagues at the RTU Institute of Silicate Materials and the Latvian State Institute of Wood Chemistry for their technical and financial support.

Finally, I would like to thank my family members for their understanding and moral support during the doctoral studies.

https://doi.org/10.7250/9789934226007
ISBN 978-9934-22-599-4 (print)
ISBN 978-9934-22-600-7 (pdf)

DOCTORAL THESIS PROPOSED TO RIGA TECHNICAL UNIVERSITY FOR THE PROMOTION TO THE SCIENTIFIC DEGREE OF DOCTOR OF SCIENCE

To be granted the scientific degree of Doctor of Science (Ph. D.), the present Doctoral Thesis has been submitted for a remote defence at the open meeting of RTU Promotion Council on 25 March 2021 14.00 at the following link: https://rtucloud1.zoom.us/j/9352086644.

OFFICIAL REVIEWERS

Lead Researcher Dr. habil. sc. ing. Jānis Grabis
Riga Technical University, Latvia

Professor Dr. chem. Kestutis Baltakys
Kaunas University of Technology, Lithuania

Professor Dr. Laszlo A. Gomze,
University of Miskolc, Hungary

DECLARATION OF ACADEMIC INTEGRITY

I hereby declare that the Doctoral Thesis submitted for the review to Riga Technical University for the promotion to the scientific degree of Doctor of Science (Ph. D.) is my own. I confirm that this Doctoral Thesis had not been submitted to any other university for the promotion to a scientific degree.

Māris Rundāns …….

Date: ……

The Doctoral Thesis has been written in Latvian. It consists of an Introduction; 3 chapters; Conclusions; 47 figures; 7 tables; the total number of pages is 92, including appendices. The Bibliography contains 109 titles.

CONTENTS

GENERAL OVERVIEW 5
Research Topicality 5
The Aim of the Thesis 5
Tasks to Be Carried Out 6
Novelty and Practical Significance 6
Thesis to Be Defended 6
Approbation of Work 7
List of publications 7
Participation in scientific conferences 8
Patent of the Republic of Latvia 9
ACRONYMS 10
1. LITERATURE REVIEW 11
2. EXPERIMENTAL METHODOLOGY 15
2.1. Development of Ceramic Material 15
2.2. Research Methods 16
3. RESULTS AND EVALUATION 19
3.1. Justification and Characterization of the Choice of Raw Material Mixture 19
3.2. Characterization of the Structure of Ceramic Materials 21
3.3. Mechanical Properties 29
3.4. Thermal properties 30
CONCLUSIONS 34
REFERENCES 36

GENERAL OVERVIEW

Cordierite is a naturally occurring magnesium aluminosilicate discovered as a natural mineral in 1813 by French geologist Louis A. Cordier. The first crystals of synthetic cordierite were obtained at the end of the 19th century (in 1899) by Polish mineralogist Joseph Morozewicz. The name ‘cordierite’ for this mineral was later suggested by English naturalists George A. Rankin and Herbert E. Merwin. It is in their work (The Ternary System MgO-Al_2O_3-SiO_2, 1918) that for the first time it is correctly placed in the $MgO/Al_2O_3/SiO_2$ phase diagram, which at the same time gives its classical chemical or stoichiometric composition as $2MgO{\cdot}2Al_2O_3{\cdot}5SiO_2$.

Over time, it was found that cordierite crystals form various polymorphic modifications both thermodynamically stable and unstable. The increasing interest in this mineral can be explained by its extremely low coefficient of thermal expansion which varies depending on the composition of the material, the volume fraction of pores, and the presence of other phases, but usually in the range of $1 \cdot 10^{-6}\ °C^{-1}$ to $4 \cdot 10^{-6}\ °C^{-1}$.

Typically, cordierite ceramics contain more than 80 % of the crystalline phase of cordierite as well as a number of other phases containing magnesium, aluminum or silica. Such ceramics have a high fire resistance, as well as its low coefficient of expansion gives shape stability even in thermally and mechanically difficult conditions. The cordierite also has suitable electrical properties that would allow it to be used as a replacement for the currently used corundum electrical components.

Research Topicality

For the use of cordierite ceramics to be economically feasible, ways to improve its production are needed. The synthesis temperature of cordierite ceramics, obtained from simple oxides, is quite high, reaching even 1450 °C.

Consequently, intensified research is underway to replace all or part of the synthetic raw materials and/or to reduce the required synthesis temperature by using various raw materials of natural origin with magnesium, aluminum and silicon oxides content.

In this work, the possibilities of obtaining cordierite ceramics using natural raw materials of local origin – clays and sand, have been studied, partially replacing the necessary synthetic raw materials. The paper describes the production of porous cordierite ceramics depending on the parameters of the synthesis process. These ceramic materials are also described from physical-mechanical, structural and thermal aspects.

The Aim of the Thesis

The aim of the Doctoral Thesis is to develop pore-containing cordierite ceramics applying Latvian mineral raw materials – illite clays and quartz sand, in the starting composition mixtures, thus obtaining a material with improved thermal and mechanical properties in comparison with traditionally obtained cordierite ceramics.

Tasks to Be Carried Out

1. Develop starting powder compositions from mixtures of mixed mineral/synthetic raw materials for obtaining cordierite ceramics.
2. Analyze the course of material synthesis by differential thermal analysis. Evaluate the possible optimal synthesis conditions (synthesis temperature, time, raw materials) for obtaining cordierite ceramics.
3. Characterize the structure of the obtained materials by X-ray diffraction, pore volume/density determination and microscopic analysis methods.
4. Determine the physical-mechanical properties of the material: compressive strength, flexural strength, modulus of elasticity.
5. Determine the parameters of thermal properties of the material: linear coefficient of thermal expansion and thermal conductivity.
6. Study the effect of cyclic thermal shock on the integral structural stability of the obtained material.

Novelty and Practical Significance

The work shows the production process of porous cordierite ceramic materials from commonly used raw materials of locally obtained quartz sand and illite clay. For the first time, a porous cordierite ceramic material was obtained without using additional fluxes or pore-forming additives, moreover, with a reduced required firing temperature compared to the technologies for obtaining analogous materials described in the literature. The physico-mechanical and thermal properties of such material, which is comparable or better than analogous materials, have been studied in depth. The importance of the work is also confirmed by the obtained Latvian patent.

Thesis to Be Defended

1. By using mineral raw materials as substitutes for synthetic components, it is possible to obtain a porous ceramic material containing the crystalline phase of cordierite by dry pressing and firing techniques.
2. By replacing the synthetic raw materials with 33 % by weight of illite clay in the starting mixtures, it is possible to lower the crystallization temperature of cordierite which, compared to the composition without clay additive, allows to lower the firing temperature of ceramics.
3. By following the synthesis process and conditions described in the work, it is possible to obtain highly porous ceramics with improved mechanical and thermal properties (compared to the traditionally obtained cordierite ceramics described in the scientific literature) which are determined by the structure formation process in this ceramic from mixtures of mineral and synthetic raw materials.

Approbation of Work

The results of work have been presented in 13 scientific conferences, published in 11 SCI listed publications, and 1 Patent of the Republic of Latvia has been obtained.

List of publications

1. Rundāns, M., Šperberga, I., Stinkulis, G. Minerālo piedevu un izejvielu dispersitātes ietekme uz kordierīta keramikas īpašībām. RTU zinātniskie raksti. 1. sēr., Materiālzinātne un lietišķā ķīmija, 2012, vol. 26, pp. 69–76 (in Latvian).
2. Rundans, M., Sperberga, I., Sedmale, G., Stinkulis, G. Effect of Sintering Process and Additives on the Properties of Cordierite Based Ceramics. IOP Conference Series: Materials Science and Engineering, 2013, vol. 47, pp. 1–5, Available: doi:10.1088/1757-899X/47/1/012012 (SCOPUS).
3. Rundans, M., Sperberga, I., Sedmale, G., Vecstaudza, D., Muter, O. Influence of bacteria Pseudomonas Fluorescens on the properties of Latvian Clay. Key Engeneering Materials, 2014, vol. 604, pp. 208–211, Available: doi:10.4028/www.scientific.net/KEM.604.208 (SCOPUS).
4. Rundāns, M., Šperberga, I., Sedmale, G. High Temperature Porous and Dense Ceramic from Latvian Quaternary Clay. Latvijas derīgie izrakteņi, jaunas tehnoloģijas, materiāli un produkti. Riga. RTU Press, 2014, pp. 81–86 (in Latvian).
5. Rundans, M., Sedmale, G., Sperberga, I., Pundiene, I. Development of Cordierite Ceramics from Natural Raw Materials. Advances in Science and Technology, 2014, vol. 89, pp. 94–99, Available: doi:10.4028/www.scientific.net/AST.89.94.
6. Rundans, M., Sperberga, I. Porous Cordierite Ceramics from Natural Clays. Material Science and Applied Chemistry, 2015, vol. 32, pp. 33–38, Available: doi:10.1515/msac-2015-0006.
7. Rundans, M., Sperberga, I., Sedmale, G. Porous and Dense Cordierite Ceramic from Illite Clay. IOP Conference Series: Materials Science and Engineering, 2016, vol. 123, iss. 1, pp. 012042–012045, Available: doi:10.1088/1757-899X/123/1/012042 (SCOPUS).
8. Rundans, M., Sperberga, I. Evaluation of Thermal Shock Influence on Cordierite Using Impulse Excitation Technique and Dynamic Mechanical Analysis. Key Engineering Materials, 2017, vol. 721, pp. 306–310, Available: doi:10.4028/www.scientific.net/KEM.721.306 (SCOPUS).
9. Sedmale, G., Randers, M., Rundans, M., Seglins, V. Application of Differently Treated Illite and Illite Clay Samples for the Development of Ceramics. Applied Clay Science, 2017, vol. 146, pp. 397–403, Available: doi:10.1016/j.clay.2017.06.016 (SCOPUS).
10. Rundans, M., Sedmale, G., Krumina, A., Ivdre, A. Influence of Technological Parameters on Thermal Properties of Cordierite Ceramics. Key Engineering Materials, 2018, vol. 762, pp. 300–305, Available: doi:10.4028/www.scientific.net/KEM.762.300 (SCOPUS).

11. Sedmale, G., Rundāns, M., Randers, M., Šperberga, I., Cimmers, A. Mineral Raw Materials of Latvia for Development of Eco-Ceramics. Materials Sciences and Applied Chemistry / Materiālzinātne un lietišķā ķīmija, 2018, vol. 35, iss. 1, pp. 62–85, Available: doi:10.7250/msac-2018-0003.

Participation in scientific conferences

1. Rundans, M., Sperberga, I., Sedmale, G., Stinkulis, G. Effect on Mineral Raw Material Addition on the Properties of Cordierite Based Ceramics. 2nd International Conference on Competitive Materials and Technology Processes, IC CMTP 2, Miskolc, Hungary, October 8–12, 2012.
2. Rundans, M., Sperberga, I., Sedmale, G., Stinkulis, G. Sintēzes proces un Latvijas minerālo piedevu ietekme uz kordierīta keramikas īpašībām. University of Latvia 71st Scientific Conference, Riga, Latvia, January 31, 2013.
3. Rundans, M., Sperberga, I., Sedmale, G., Vecstaudza, D., Muter, O. Influence of Bacteria Pseudomonas Fluorescens on the Properties of Latvian Clay. 22nd International Baltic Conference of Engineering Materials & Tribology – BALTMATTRIB 2013, Riga, Latvia, November 14–15, 2013.
4. Rundans, M., Sperberga, I., Sedmale, G. Augsttemperatūras poraina keramika no Latvijas minerālajām izejvielām. University of Latvia 72nd Scientific Conference. Earth and Environmental Sciences. Geology, Riga, Latvia, January 31, 2014.
5. Sedmale, G., Sperberga, I., Rundans, M., Grase, L. Different Treatment Application of Illite Clay for Low Temperature Ceramics. 13th International Ceramics Congress – CIMTEC 2014, Montecatini Terme, Italy, June 8–13, 2014.
6. Rundans, M., Sperberga, I., Sedmale, G. Porous and Dense Cordierite Ceramic from Illite Clay. 3rd International Conference on Competative Materials and Technology Processes, Miskolc, Hungary, October 6–10, 2014.
7. Rundans, M., Sperberga, I., Sedmale, G. Poraina kordierīta keramika ar Latvijas Kvartāra mālu. University of Latvia 73rd Scientific Conference. Earth and Environmental Sciences. Geology, Riga, Latvia, February 6, 2015.
8. Rundans, M., Sperberga, I. Thermal Shock Influence on the Mechanical Strength of Cordierite Composite Ceramics. University of Latvia 74th Scientific Conference: International and Interdisciplinary Symposium «Clays and Ceramics», Riga, Latvia, January 28–29, 2016.
9. Rundans, M., Sperberga, I. Evaluation of Thermal Shock Influence on Cordierite Ceramics Using Different Testing Methods. 25th International Baltic Conference of Engineering Materials & Tribology – BALTMATTRIB 2016, Riga, Latvia, November 3–4, 2016.
10. Rundans, M., Sedmale, G., Krumina, A., Ivdre, A. Influence of Technological Prameters on Thermal Properties of Cordierite Ceramics. Material Science and Applied Chemistry (MSAC 2017), Riga, Latvia, October 20, 2017.

11. Rundans, M., Sedmale, G., Grase, L. Porous Cordierite Ceramics with Illite Clay Additive: Synthesis and Properties. 8th International Conference on Silicate Materials BaltSilica 2018, Riga, Latvia, May 30 – June 1, 2018.
12. Rundans, M., Sedmale, G., Grase, L. Impact of Illite Clay and Sintering Conditions on Development of Porous Cordierite Ceramics. 14th International Ceramics Congress – CIMTEC 2018, Perugia, Italy, June 4–14, 2018.
13. Rundans, M., Sedmale, G., Grase, L., Svinka, R. Mechanical and Thermal Properties of Porous Cordierite Obtained from Natural Raw Materials. 5th International Conference on Competative Materials and Technology Processes, Miskolc, Hungary, October 8–12, 2018.

Patent of the Republic of Latvia

1. LV15314B, 20.05.2018., Temperature Shock-Resistant Porous Cordierite Ceramic. M. Rundāns, G.M. Sedmale, I. Šperberga.

ACRONYMS

CTE, α – thermal expansion coefficient;
ρ_s – electric resistivity;
ε – dielectric constant;
σ_f – flexural strength;
σ_c – compressive strength;
E – elastic modulus;
E_0 – theoretical elastic modulus;
E_d – elastic modulus in dynamic mechanic analysis mode;
E_f – elastic modulus in three-point flexure mode;
r – Pearson correlation coefficient;
K_{Ic} – plane strain fracture toughness;
DMA – dynamic mechanical analysis;
SEM – scanning electronmicroscopy;
DTA – differential thermal analysis;
BET – Brunauer–Emmett–Teller (theory);
a – thermal diffusion;
λ – thermal conductivity;
c_p – specific heat.

1. LITERATURE REVIEW

Mineral cordierite is a compound of three components – MgO, Al_2O_3 and SiO_2 – magnesium aluminosilicate which, based on its structure, can be classifief into tectosilicates, in the same group with zeolites. In the $MgO–Al_2O_3–SiO_2$ ternary system, the stoichiometric point of cordierite corresponds to the composition of $2MgO·2Al_2O_3·5SiO_2$. The stoichiometric weight ratio of cordierite oxides corresponds to 13.7 % MgO, 34.9 % Al_2O_3 and 51.4 % SiO_2. Its formula unit corresponds to composition $Mg,X[Al_4Si_{10}O_{18}]$, where X is a divalent metal ion, which in nature is most often Fe^{2+}, but it is also possible for it to be replaced with other divalent iron group ions such as Co^{2+}, Ni^{2+}, Cu^{2+}. Other cations (Na^+, K^+, Be^{2+}, Ca^{2+}, Mn^{2+}, etc.) and volatile compounds (H_2O, CO_2, Ar, etc.) may also be present in small amounts in the structure of cordierite [1, 2].

The crystalline phase of cordierite melts incongruently between 1440–1460 °C, decomposing into mullite and liquid phases, while complete melting occurs at 1550 °C [3–6]. Cordieritis is characterized by a complex polymorphism dominated by two thermodynamically stable (α- and β-cordierite) as well as metastable forms. Cordierite α- and β-modifications are stable over a sufficiently wide range of ambient pressures and temperatures [3, 7–9], so both polymorphs are equally common in natural rocks.

The modification of α cordierite is called indialite (Fig. 1.1) – the designation originated because this phase was first found in a sample of cordierite mineral found in India [10]. Indialite forms crystals of hexagonal system and its symmetry of the crystal lattice corresponds to the spatial group P6/mcc (No. 192), moreover, this form is considered to be isotypic with the mineral beryl ($Be_3Al_2Si_6O_{18}$) [11], in turn, the crystals of the polymorphic modification of β-cordierite (Fig. 1.2) represent rhombic syngony (Cccm spatial group No. 66). Both α- and β-cordierite microstructures consist of ring-linked $[AlO_4]^{5–}$ and $[SiO_4]^{4–}$ tetrahedral structural elements which are alternately connected to each other forming a three-dimensional, hollow cylindrical structure in the parallel direction of the crystallographic c-axis. The rings are bonded and electron neutrality is ensured by octahedral cations of Mg^{2+} (or other divalent metals). The channel symmetry of the indialite structure is close to an ideal regular hexagon [5], and its structure is composed of disordered Al/Si tetrahedra in its $(Si, Al)_6O_{18}$ rings, while the β-cordierite structure has an ordered ring structure in which Si–O and the Al–O ratio is fixed; Si–O tetrahedra in β-cordierite structure are located in 3 different positions but Al–O – in two. Thus, one β-cordierite ring structure consists of four Si–O and two Al–O tetrahedra, while the rings are interconnected by four Al–O and two Si–O tetrahedra. Unlike the indialite structure, the low-temperature cordierite ring system is symmetrically deformed, so that the hollow channels are slightly elliptically curved in a direction perpendicular to the c-axis. The presence of small molecule compounds and alkali metal cations is also more common in β-cordierite structure than in the indialite crystals [12].

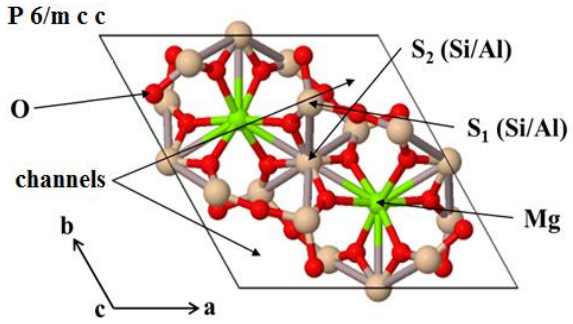

Fig 1.1. Indialite (α-cordierite) structure. S_1 – channel-forming Si/Al tetrahedra, S_2 – structure-forming Si/Al tetrahedra.

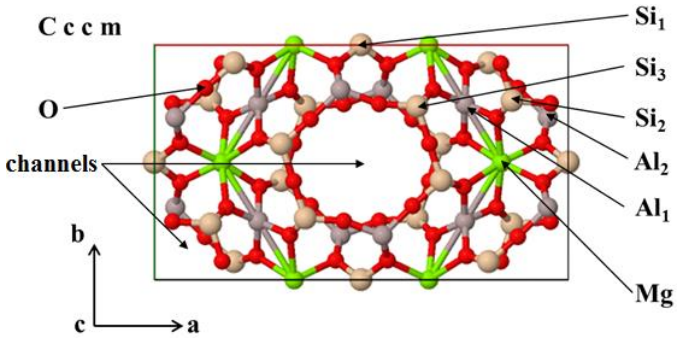

Fig. 1.2. Low-temperature β-cordierite structure: Si_1, Si_2 and Al_1 – structure-forming Si/Al tetrahedra; Si_3 and Al_2 – channel-forming Si/Al tetrahedra.

Indialite is often considered to be the most thermodynamically stable modification, so it is usually formed when cordierite is obtained synthetically by the solid phase synthesis method [3], as well as when there is crystallization of glassy melts corresponding to stoichiometric composition of cordierite in temperature range 1000–1300 °C. In hydrothermal synthesis, indialite crystals are formed at temperatures above 830 °C [10]. β-cordierite is stable under normal conditions, but when heated at temperatures above 1000 °C, β-cordierite is converted to α-cordierite in the presence of liquid phase [3, 13]. However, the polymorphic transition of α/β-cordierite is reversible, and according to [11], it follows the order-disorder transition mechanism, which involves both structure and ring-forming Si/Al-O tetrahedra.

Artificial synthesis of cordierite is the most common way of obtaining it, and it is performed by various methods. The need for synthetic acquisition of cordierite is determined by its rare prevalence in nature, which in turn means that the mining of cordierite from deposits containing it for technical purposes is not economically viable.

There are several methods for synthesizing cordierite such as solid phase reactions, sol-gel process, and crystallization from glass melts. Among these methods, the most commonly used is high-temperature solid-phase reactions to obtain cordierite from a mixture of stoichiometric oxide powders of MgO, Al_2O_3 and SiO_2 at temperatures well above 1350 °C [8]. The raw materials used are synthetically produced magnesium, aluminum and silicon oxides as well as natural raw materials, the most commonly used of which are talc ($3MgO{\cdot}4SiO_2{\cdot}2H_2O$), kaolinite ($Al_2O_3{\cdot}2SiO_2{\cdot}2H_2O$) and quartz sand ($SiO_2$). In addition, other materials of natural origin are used, such as potassium feldspar

($KAlSi_3O_8$), forsterite ($2MgO \cdot SiO_2$), sepiolite ($4MgO \cdot 6SiO_2 \cdot 8H_2O$), magnesite ($MgCO_3$), andalusite ($SiAl_2O_5$), stevensite ($Si_4Mg_3O_{10}$), etc. [14–16].

Both high-temperature and low-temperature cordierite ceramic materials have a distinctly low coefficient of thermal expansion (CTE, α) along the crystallographic c-axis, which is related to the structure of the predominantly strong covalent bonds in the structure [11, 17]. The mentioned (practically determined and/or theoretical) CTE values in the literature vary in a rather wide range, e.g., $\alpha_{cord.} \approx 1.5 \cdot 10^{-6}$ °C^{-1} to $4.0 \cdot 10^{-6}$ °C^{-1} [18]. It naturally follows that ceramics with the maximum low (close to zero value) total CTE are particularly resistant to rapid temperature changes, e.g., the product is heat shock resistant. It is assumed that the critical temperature difference between pure cordierite ceramics at which cracks are formed as a result of thermal shock is ΔT_c = 300–350 °C, and cracks are formed only within 2–3 seconds from the start of rapid cooling/heating [19].

The presence of most other phases in cordierite ceramics increases its overall CTE value, but the effect of these phases on other important ceramic properties, such as thermal shock resistance, mechanical strength, dielectric permittivity, etc., differs, so sometimes individual phases in cordierite ceramics are deliberately formed (e.g., mullite) [20].

In addition to low CTE values, cordierite ceramic materials can also be characterized by quite good physical-mechanical parameters which determine the areas of practical application. Some of the most important physical-mechanical and electrical properties of cordierite ceramic materials are given in Table 1.1.

Table 1.1

Some Physical-Mechanical Parameters of Cordierite

Parameter	**Denotation**	**Value**
Plane strain fracture toughness	K_{Ic}	1.65–2.90 MPa·m$^{1/2}$ [21]
Flexural strength of polycrystalline cordierite	$\sigma_{f\_pract.}$	88.1 MPa [22]
Flexural strength of single crystal cordierite	$\sigma_{f\_theor.}$	245 MPa [23]
Theoretical modulus of elasticity	E_0	134 GPa [24]
Dielectric constant	ε	4–6 [20]
Electrical resistivity	ρ_s	10^{12} Ω·cm [20]

Compared to other high-temperature materials, the physical-mechanical properties of cordierite can be considered as average. Table 1.1 shows values for absolutely dense cordierite ceramics, but almost all properties are determined not only by the content of pores (porosity) but also by the pore distribution, size and shape. The flexural strength of monophasic cordierite ceramics is σ_f = 45–50 MPa at approximately 8 % porosity, but if porosity is reduced to 4.5 %, σ_f increases to 50–53 MPa [19]. Cordierite ceramics show better results in compressive strength tests (up to $\sigma_c \approx 550$ MPa for dense product), which improves if the ceramic contains SiO_2-rich glassy phase but deteriorates if the structure is

inhomogeneous and/or porous – compressive strength decreases on average down to 100 MPa if the porosity exceeds 20 % [25].

The use of cordierite ceramics derives from its properties. Its low CTE as well as its chemical, physical and thermal resistance is the reason for its use in high temperature (>1000 °C) conditions as a substrate for exhaust gases, molten metal filters and catalytic converters [6]. Low dielectric constant and high specific electrical resistance make it possible to replace corundum (Al_2O_3) products in microelectronics with cordierite ceramics [20], e.g., used as a chip substrate element in combination with silicon components. For simpler purposes, cordierite ceramics are used as high temperature and chemically resistant substrates in chemical laboratories. The production of all products is facilitated by the possibility to make cordierite ceramics from natural materials, which reduces production costs, but in this way deviations from the theoretically possible properties of ceramics due to both impurities in raw materials and production conditions must be taken into account. Research showing the practical application of the obtained cordierite materials is the main goal of many scientific works [14, 22, 25, 26].

2. EXPERIMENTAL METHODOLOGY

2.1. Development of Ceramic Material

Two illite-type clays from Apriķi and Nīcgale deposits were used to obtain cordierite ceramic materials. The chemical and granulometric composition of both clays is shown in Table 2.1.

Table 2.1

Chemical and Granulomteric Composition of Apriķi and Nīcgale in wt. %

Clay	**SiO_2**	**Al_2O_3**	**MgO**	**CaO**	**Fe_2O_3/TiO_2**	**Na_2O/K_2O**	**LOI***
Apriķi	53.0	15.8	2.8	6.4	6.0	3.9	12.1
Nīcgale	51.0	16.5	2.4	6.8	6.3	5.0	11.4
Fraction:		<2 μm		2–63 μm		>63 μm	
Apriķi		84.7		13.4		1.9	
Nīcgale		67.5		32.1		0.4	

* loss on ignition.

Mixtures with both of these clays were obtained by stoichiometric mixing of $MgCO_3$, $Al(OH)_3$, ground quartz sand (Bāle deposit, >99.0 % pure) and the above clays; a mixture without clay content (K0) was also prepared as a reference composition (Table 2.2). The clay content in the mixtures was selected by evaluating the results obtained in preliminary tests (not included in the work). All raw mixtures were homogenized by grinding in a planetary mill for two hours. Distilled water was used as the grinding medium, with a dry weight ratio of approx. 1.0:1.5. The slurries obtained after milling were dried at 100 °C till constant weight.

Table 2.2

Compositions of Starting Powders in wt. %

Powder ID	**$MgCO_3$**	**$Al(OH)_3$**	**SiO_2 (sand)**	**Clay**
A5 (Apriķi clay)	17.0	27.0	23.0	33.0
N5 (Nīcgale clay)	16.5	26.0	24.5	33.0
K0 (no clay additive)	21.5	34.4	44.1	–

The obtained dry powders were compacted using the dry pressing method into rectangular steel molds. The pressing was performed with a hand press and the pressing pressure was ≈200 bar (20 MPa).

The samples obtained after compacting were fired in a muffle furnace under normal atmosphere and pressure. The rate of temperature rise in all cases was 6 °C/min. The maximum holding time and the maximum holding temperature were varied. The holding time

was changed from 1 to 3 hours. The control (K0) sample was fired at 1400 °C and kept at maximum temperature for 3 hours. For compositions with clay content, the maximum temperature was changed from 1200 °C to 1350 °C, in the range from 1250 °C to 1350 °C the temperature was changed every 25 °C (as a result, samples A5 1250, A5 1275, A5 1300, etc. were obtained). After cooling, the fired samples were cut with the help of a fine diamond cutting disc (disc thickness – 0.4 mm), depending on the dimensions of the samples required for the specific testing purpose. A schematic development process of the cordierite ceramic samples is shown in Fig. 2.1.

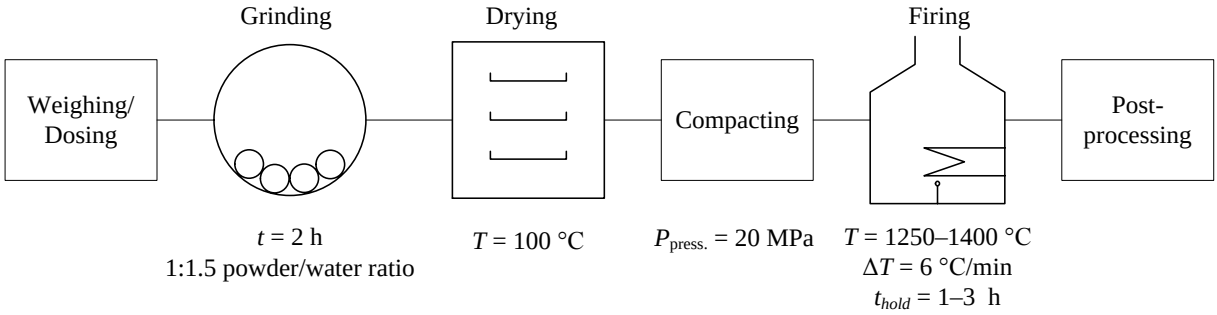

Fig. 2.1. General scheme of obtaining cordierite ceramic samples.

2.2. Research Methods

The degree of dispersion of the raw materials was determined by means of laser granulometry using a *CILAS 930 Particle Size Analyzer* which measures the size distribution of particles with a diameter of 0.2 μm to 500 μm. The surface areas of the starting powders were characterized by nitrogen adsorption (BET method) (*Quantachrome Instruments Pore Size Analyzer Nova 1200E*), but the processes that took place during the synthesis (decomposition, melting, crystallization) from room temperature to 1400 °C – by differential thermal analysis (DTA) using *SETSYS Evolution TGA-DTA/TMA SETARAM* equipment under inert environment with corundum as reference material.

The ceramic properties (water absorption, bulk density and apparent porosity) of the synthesized cordierite materials were determined using the Archimedes' hydrostatic weighing method. The porosity of the samples was also characterized by mercury intrusion porosimetry (*Quantachrome Instruments Pore Master 33*) of small (effective diameter <1 cm) ceramic shards. The composition of the crystalline phases in the powdered ceramic samples was determined using *Bruker D8 Advance X-Ray* equipment. CuKα radiation source (λ = 0.15406 nm) was used; the X-ray diffraction pattern was taken at a speed of 4 °/min in the range of two theta (2θ) angles from 5° to 60°. Quantitative phase composition was calculated using Riedveld analysis.

The surface analysis of the samples was performed using a stereomicroscope *Zeiss SteREO Discovery V12* as well as scanning electron microscopes *FEI Nova NanoSEM 650* and *Hitachi TableTop Microscope TM3000*. The surface condition of individual samples was improved by polishing and chemical (10 % HF solution) etching.

The maximum compressive strength for cubic specimens with a height:length:width ratio of approx. 1:1:1 was determined by applying a continuously increasing load perpendicular to

the flat parallel surfaces of the test specimen up to its point of failure with the *Compression Test Plant ToniNorm, ToniTechnik by Zwick (200 kN)*. The *Static Materials Testing Machine Zwick/Roell Z010 TN (100 kN)* equipped with a non-contact extensometer and the testXpert II software were used to determine the maximum flexural strength (breaking point) and modulus of elasticity of the specimens. The test specimens for flexural strength tests were rectangular parallelepiped-shaped specimens with approximately 90:8:6 length, width, and thickness (complying with ASTM C1161) ratio. In parallel, the modulus of elasticity was determined by dynamic mechanical analysis (*Mettler Toledo DMA/SDTA 861e*). The samples were in the form of rectangular parallelepipeds approx. 40 mm × 12 mm × 3 mm in length, width and thickness. The 'fixed-end' method was used in a three-point configuration, and the samples were tested in four different harmonic oscillation modes (0.1 MHz, 1 MHz, 10 MHz and 100 MHz).

The horizontal push-rod dilatometer *Linses L67 Platinum Series* was used for dilatometric studies. Rectangular parallelepiped-shaped specimens with approximate dimensions of 20 mm × 5 mm × 5 mm (length/width/height) were used. Quartz was used as the push-rod material. Dilatometric curves were recorded in the range of 20–1000 °C with a heating rate of 10 °C/min.

The thermal conductivity of the samples in the temperature range from 20 °C to 600 °C was determined by the laser flash analysis method using thin square plates (approx. 10 mm × 10 mm × 2 mm) coated with a thin (<0.1 mm) homogeneous layer of graphite to prevent heat dissipation.

The effect of cyclic thermal shock on the obtained samples was determined according to a modified ASTM C1525 method. The testing process is shown schematically in Fig. 2.2.

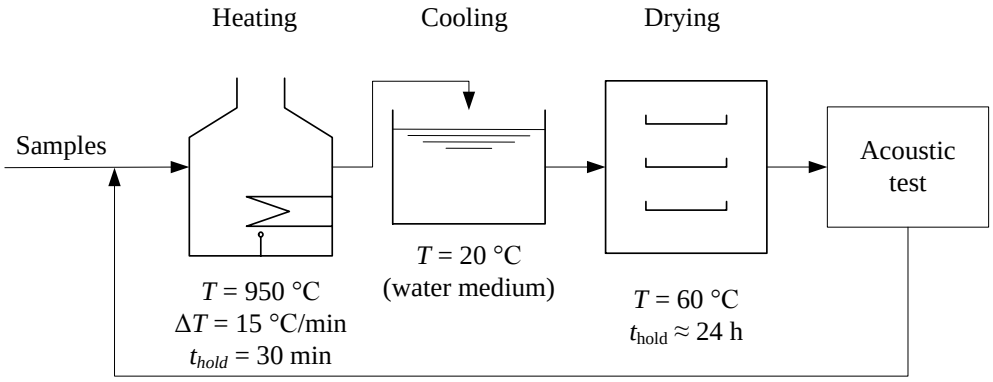

Fig. 2.2. Cyclic thermal shock impact test scheme.

Changes in the integrity of the dried samples were recorded by determining the changes in their dynamic Young's modulus of elasticity by the acoustic impulse excitation method. The modulus of elasticity was determined using the *Buzz-o-Sonic 5.0* system: a rectangular sample (40 mm × 12 mm × 3 mm) was placed on triangular pieces of polyurethane sponge at its resonance points corresponding to 0.224*l* distances from the sample ends. The acoustic impulse in the middle of the test sample was induced by a steel ball attached to a polyethylene holder. From the obtained acoustic signal, the modulus of elasticity at the most intense

resonant frequency in the obtained spectrum was calculated. All calculations were performed assuming a Poisson's ratio of 0.3 for the material.

For all measurements in which more than one parallel sample was tested (ceramic and mechanical properties), the measurement error values were determined using the statistical analysis function STDEV of the *Microsoft Excel* program. The obtained values are displayed (wherever visually meaningful) as error limits in the graphs of the respective results.

3. RESULTS AND EVALUATION

3.1. Justification and Characterization of the Choice of Raw Material Mixture

Two base compositions A5 and N5 have been used for the development of porous cordierite ceramics, which differ from the traditionally used compositions for the synthesis of cordierite mainly by the presence of two types of easily melting illite clays (clay from Apriķi and Nicgale deposits). These clays are characterized by quite similar chemical composition – the weight ratio of their two main components SiO_2 and Al_2O_3 ranges from 3.25 to 3.10, as well as they have a relatively high Fe_2O_3 content – about 6.0–6.3 %. The main difference between these clays is related to the composition of their mineralogical fractions. Both have a clay mineral fraction represented by illites with a small impurity of kaolinite or chlorites. In turn, the amount of this fraction is quite different in each of them – the amount of clay mineral fraction in Apriķi clay is estimated at about 86 %, while in Nīcgale clay about 73 % [27]. It should also be noted that the silt fraction is different as well, which is mainly represented by carbonate-containing minerals – in Apriķi clay it is estimated on average about 11.7 %, but in Nīcgale clay about 22.0 %. In general, the presence of clays in ceramic raw material mixtures, especially the clay mineral fraction, is the main reason for the formation of the liquid phase in the firing process and thus to the easening of the sintering process. They also have a significant role in the formation of intended crystalline, as well as glassy and gaseous phases. The presence of $MgCO_3$, $Al(OH)_3$ as well as quartz sand, after their transformation in the firing process, mainly provides the required stoichiometry for the raw composition to form the main – cordierite crystalline phase.

The characterization of the particle distribution of raw materials obtained by the laser granulometry method is shown in Table 3.1. Laser granulometry provides statistically complete and direct information on the particle size distribution of mixtures.

Table 3.1

Ground (Sand, N5, A5) and Unground (Clay) Raw Material Granulometry Results in μm

	Ground quartz sand (20 h)	**Nīcgale clay**	**Apriķi clay**	**Ground N5 (2 h)**	**Ground A5 (2 h)**
Average particle size (median)	14.0	6.0	5.0	16.3	15.8
Interquartile range	20.0	8.1	7.8	24.5	23.4

The average particle size of N5 and A5 in the basic composition of the raw material mixture is approximately 5.0–6.0 μm for clay, but the particle size of the prepared basic compositions is 15.8–16.3 μm. As a result of grinding, the average particle size for compositions N5 and A5 has increased, on average, 2.6 times in relation to the size of clay particles, but practically has not changed in relation to the Quartz sand raw material (Table 3.1). Thus, it can be concluded that the dispersion of the starting compositions is

mainly determined by the degree of fineness of the coarsest (sand) raw material. The specific surface area determined by the nitrogen absorption analysis method for raw materials and ground compositions is shown in Table 3.2.

Table 3.2

Specific Surface Area (*S*) of Raw Materials and Powders in m^2/g

$MgCO_3$	$Al(OH)_3$	Quartz sand	Nīcgale clay	A5	N5	K0
29.4 ± 0.1	24.7 ± 0.1	1.2 ± 0.1	24.3 ± 0.1	3.4 ± 0.1	3.5 ± 0.1	1.6 ± 0.1

As shown in Table 3.2, both clay powders as well as synthetic raw materials [$MgCO_3$ and $Al(OH)_3$] have a relatively high specific surface area, while the specific surface area of sand remains low, which reduces the specific surface area of the starting mixtures A5 and N5 to, on average, 3.4 $m^2/g \pm 0{,}1$ m^2/g for compositions with added clay (A5 and N5) and for control sample K0 down to 1.6 m^2/g. Therefore, it must be concluded that the clay components approximately double the specific surface area of the starting mixtures, which could facilitate the sintering process.

Differential thermal analysis results for compositions N5, A5 and K0 are shown in Fig. 3.1. The basic mass loss processes take place up to about 750 °C but for a control composition (without clay additive) up to 550 °C. Endothermic effects up to 750 °C are associated, firstly, with the release of physically and chemically bound water, and secondly, with the decomposition of $Al(OH)_3$ undergoing a complex transformation process from $Al(OH)_3$ (gibbsite form) to α-Al_2O_3 (corundum form) state, formally following the reaction path $2Al(OH)_3 \rightarrow \alpha\text{-}Al_2O_3 + 3H_2O\uparrow$, in the intermediate stages forming γ-AlOOH (boemite) as well as the γ, δ, χ, θ and κ-Al_2O_3 forms [28]. It should be noted that the decomposition effects of carbonates in their characteristic temperature range around 800–900 °C were not observed in any of the compositions.

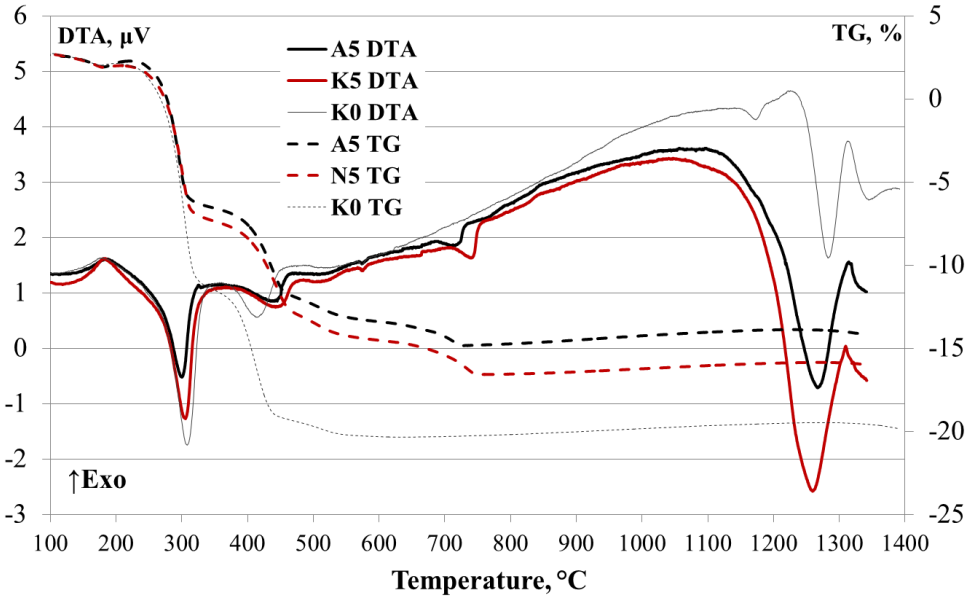

Fig 3.1. Differential thermal analysis (DTA) of compositions A5, N5 and K0.

The predominant endothermic processes in all cases take place at temperatures above 1100 °C, when the formation of the liquid phase begins to intensify. At temperatures above 700 °C, after the 'collapse' of the illite clay structure (which can also be seen in the DTA curves) and the formation of possible Ca(Mg)-Al(Fe)-Si-O micro-eutectic, relatively intensive liquid phase formation occurs. In compositions with clay additives in the temperature range from 1100 °C to 1400 °C, the degradation processes are rapid and difficult to distinguish when several processes take place simultaneously. The formation of low-temperature cordierite occurs at lower temperatures than in the control sample, which can be explained by the presence of iron compounds. As a result of chemical reduction of iron oxides after the reaction $2Fe_2O_3 \rightarrow 4FeO + O_2\uparrow$, swelling of the samples occurs as a result of the released gaseous phase, as well as visual discoloration of the samples from reddish brown to light gray due to changes in the oxidation degree of iron compounds.

However, the formation of new phases in the control sample is gradual and takes place in the range of 1200–1400 °C, where two endothermic (at 1185 °C and 1280 °C) and two exothermic effects (at 1250 °C and 1320 °C) are evident. Endothermic effects are associated with component transformation and nucleation processes, while exothermic effects are associated with the formation of β-cordierite (at lower temperature) and α-cordierite (at higher temperature). The pronounced endothermic effect between the two crystallization points is most likely related to the breakdown of low-temperature cordierite.

3.2. Characterization of the Structure of Ceramic Materials

Since the main crystallization processes of cordierite in samples A5 and N5 take place at temperatures above 1250 °C, changes in crystalline phases by X-ray diffraction have been determined for samples fired in the temperature range from 1250–1350 °C each 25 °C. According to the data shown (Fig 3.2), all fired samples are highly crystalline and contain cordierite as the major crystalline phase. Sample K0 has a similar composition (not shown).

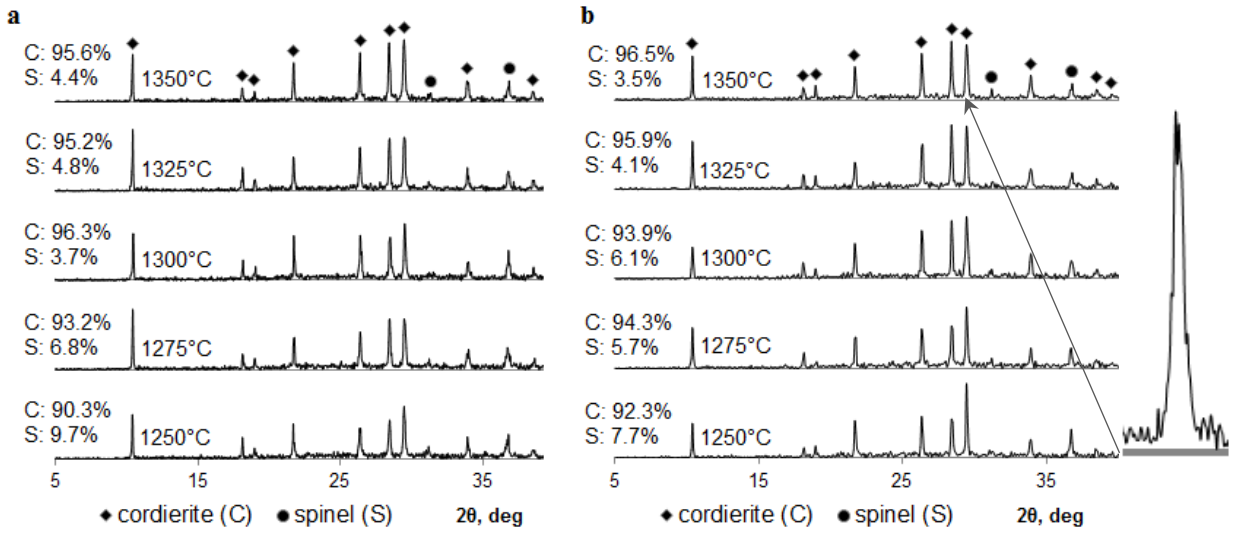

Fig 3.2. X-ray diffraction patterns for samples A5 (a) and N5 (b) after firing in 1250–1350 °C. Inlet – magnified 29–30° peak splitting.

Spinel has been found as a secondary phase in all compositions. The phases detected at lower temperatures (1200 °C, not shown) – corundum, quartz, anorthite and sapphirine at temperatures starting at 1250 °C have either been transformed by reaction into cordierite / Mg spinel compounds, or these phases have melted and are forming amorphous phases in the final product. Although the composition of the amorphous phase cannot be determined by X-ray diffraction, it is hypothesized that this phase is formed partly of K-Na-Ca-Fe compounds with SiO_2 (and possibly partly also Al_2O_3) because the presence of these elements in the form of separate crystalline phases are not found. However, Fe^{2+} is able to partially replace Mg^{2+} in the cordierite/spinel crystal structures.

Performing Rietveld refinement on all formulations and using cordierite (JCPDS # 01-089-1487) and magnesium spinel (JCPDS # 01-075-1798) model data as a reference, shows that the spinel/cordierite ratio decreases with increasing firing temperature, e.g., the spinel reacts with the silica in the amorphous phase to form the cordierite according to the reaction:

$$2MgAl_2O_4 \text{ (spinel)} + 5SiO_2 \rightarrow Mg_2Al_4Si_5O_{18} \text{ (cordierite)}$$

For composition A5, the highest cordierite/spinel ratio was found at 1300 °C. At higher temperatures the ratio decreases, indicating that the opposite reaction takes place, e.g., the cordierite decomposes into spinel and amorphous SiO_2. Also, Rietveld's analysis shows that all samples have the presence of mixed α/β cordierite crystalline phases the ratio of which cannot be quantitatively accurately determined but can be qualitatively detected by X-ray phase analysis observing peak splitting at 29–30 2θ degrees (inlet of Fig. 3.2).

Comprehensive information on the sample structure is provided by stereomicroscopy (Fig. 3.3 a–d) and scanning electron microscopy (Fig. 3.4–3.7) images.

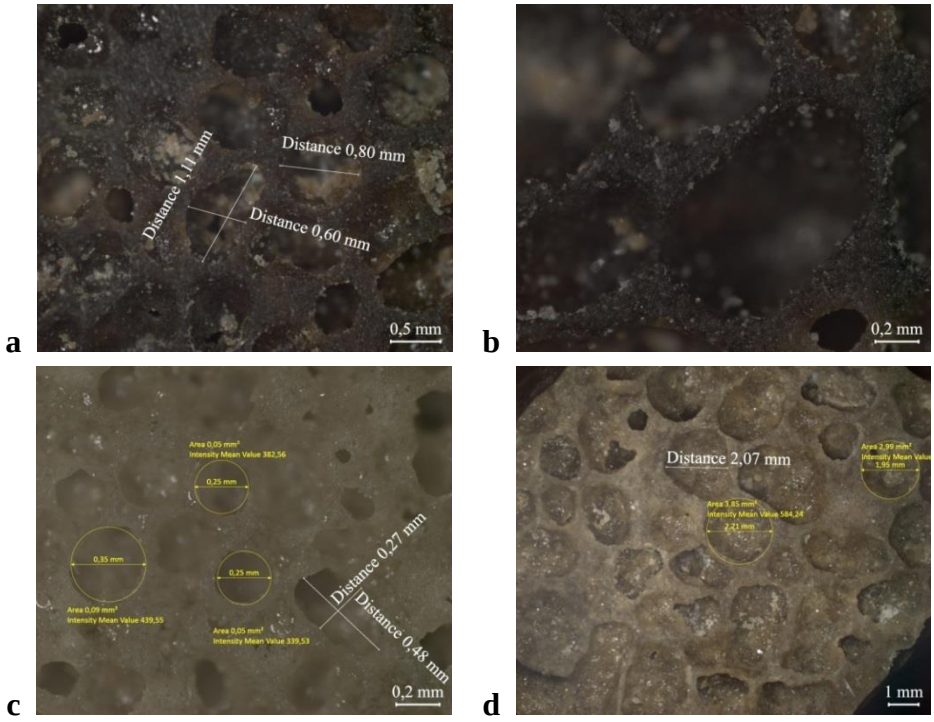

Fig. 3.3. Steroemicroscope images of cross-sectional surface of samples A5 1250 (a), A5 1300 (b), N5 1250 (c) and N5 1300 (d).

These images show that the samples can be described as mostly having closed pore system. The structure of individual pores is semi-permeable, indicated by openings in the inner surface of individual pores. The pore sizes of the samples are not uniform and strongly depend on both the composition and the firing temperature. The marks in the images give a rough idea of the effective diameter of the pores in the sample. The average estimated pore diameter of samples A5 1250 is about 0.6–1.0 mm (Fig. 3.3 a); the diameter of the pores of the samples obtained at higher temperatures (1300 °C) increases to 2.0–2.2 mm (Fig. 3.3 b), which indicates a sharp course of physicochemical processes in this temperature range. Similarly, the average pore diameter of the samples obtained at 1250 °C of samples N5 is 0.5–0.8 mm (Fig. 3.3 c), but of the samples obtained at 1300 °C – 1.9–2.1 mm (Fig. 3.3 d). The mean pore diameter of the samples obtained at the highest temperature remains practically constant, fluctuating within an average of 2.0 mm ± 0.2 mm. In addition to the type and size of the pores, the stereomicroscope images show that the sample walls are thin in relation to the pore size and are significantly lined with aggregates of vitreous mass in the form of individual aggregates both at higher and lower temperatures.

Alternative representation and information on the microstructure of the samples is provided by scanning electron microscopy (SEM) images. Figure 3.4 shows the cross-sectional macrostructure of the raw sample A5 1300 which is comparable to images obtained by stereomicroscopy. The figure shows that the sample is characterized by large (1.5–2.0 mm) pores separated by relatively narrow (<0.1 mm) pore walls.

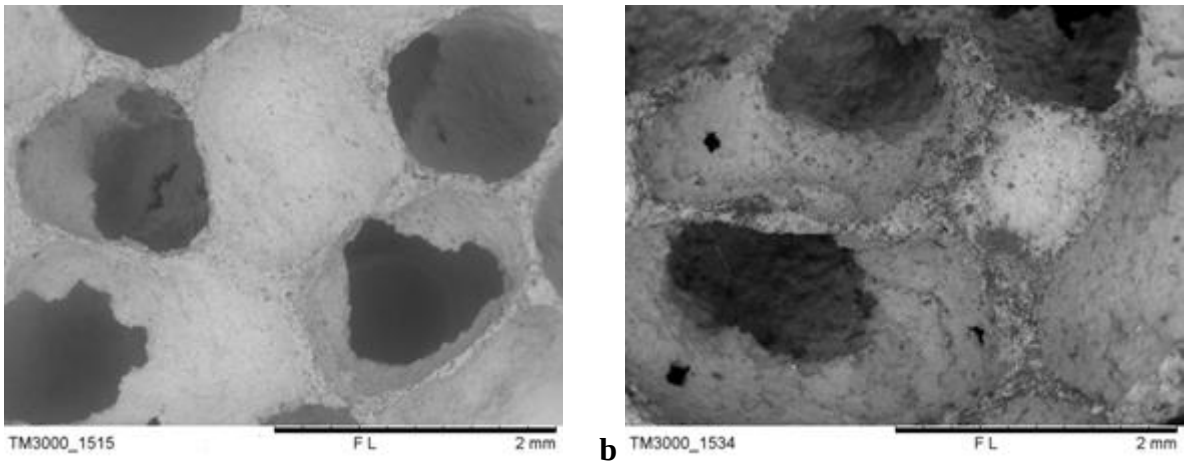

Fig. 3.4. SEM images of cross-section of samples N5 1300 (a) and A5 1300 (b).

Similar to the stereomicroscope images, semi-permeable pores are observed here, as evidenced by the darkest areas (openings) on the surface of individual pores. Unlike stereomicroscope images, SEM images do not show the presence of vitreous phase grain aggregates, which can be explained by differences in SEM and stereomicroscope image acquisition principles.

Figure 3.5 shows the structure of polished surface of samples A5 1275 (etched) and N5 1275 (non-etched). Without etching (Fig. 3.5 b) in the surface image, the crystalline/vitreous areas can be distinguished only conditionally on the basis of local tonal

differences (darker areas – crystalline cordierite/spinel phase, lighter – amorphous phase, based on the assumption that the crystalline phase contains less 'heavy' Fe, Ca, K elements, thus in SEM images these areas are relatively darker than the glassy phase which is likely to contain significantly more of these elements. In addition to the tonal differences, the fact that the darkest areas in the walls of the material are the crystalline phase is also indicated by the straight, angular shapes which are especially well visible in Fig. 3.5 a. Attention should also be paid in this sample to the pronounced hexagonal crystals, the 'empty' central part of which is surrounded by a thin layer of vitreous phase and islets of small crystalline aggregates.

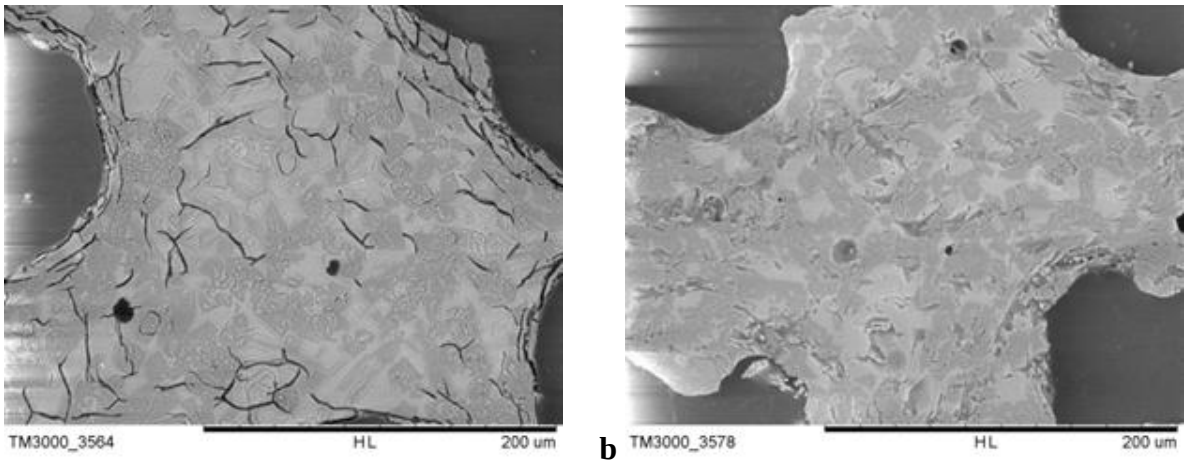

Fig. 3.5. Samples A5 1275 (a, etched surface) and N5 1275 (b, untreated surface) at 500× magnification. Darker areas – crystalline phase, lighter – amorphous.

At a larger magnification of sample A5 1275 (Fig. 3.6), it is clear that the layer surrounding the inner part of the hexagonal crystals is degraded by the etching, which directly indicates the presence of amorphous phase. Also, in the central part (Fig. 3.6 b) it can be seen that the crystalline aggregates are formed of microprismatic, unbound crystallites. Taking into account the information on the crystalline nature of α and β cordierite, it must be concluded that relatively large but centrally 'empty', crystallographically 'correct' hexagonal crystals in the walls of the material are incompletely formed α-cordierite crystals. Given the presence of a vitreous phase layer and crystal aggregates inside the large hexagons, it must be assumed that these crystalline aggregates are the initially formed 'residues' of orthorhombic β-cordierite which re-crystallize in the high-temperature α-cordierite hexagons. In this way, X-ray diffraction data on the existence of α/β-cordierite mixed phase in the material are additionally substantiated. Taking into account the results of SEM microstructure and X-ray diffraction data analysis, it is possible to hypothesize that α-cordierite is formed from β-cordierite crystals by a gradually generated glassy phase with a gradual transition to a single-phase compound. However, within the experiments, the state of single-phase material was not reached and may not be practically achievable due to the proximity of the thermal decomposition point of cordierite.

Similar to Fig. 3.6, samples obtained at higher temperatures shown in Fig. 3.7 are similar in nature. The presence of incomplete hexagonal crystallites and a significant amount of glassy phase content are also observed. It should be noted that the α-cordierite (hexagonal)

crystallites shown in these figures, more often than in lower temperature samples, exhibit deformations (are stretched/flattened), which indicates increasing spatial competition between the individual α-cordierite crystals. Similarly, the hexagonal crystallites of the samples obtained at higher temperatures are larger in size (≈30–40 μm, approx. measurement) compared to those obtained at lower temperatures (<20 μm, approx. measurement).

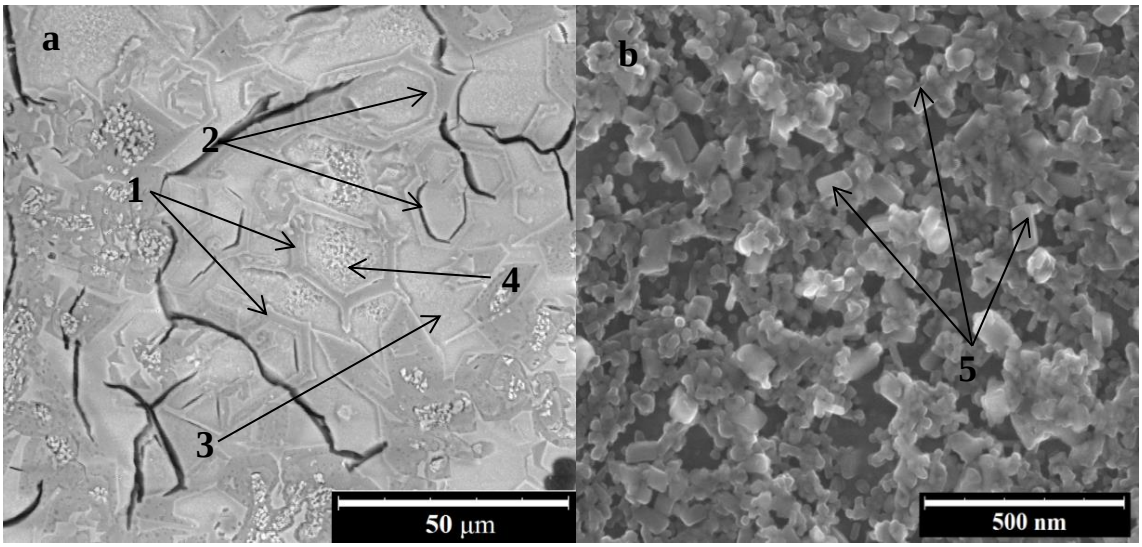

Fig. 3.6. Surface images of etched sample A5 1275, 1000× (a) and 50 000× (b) magnifications: 1 – 'empty' hexagonal crystallites; 2 – secondary generated amorphous interphase; 3 – primary amorphous phase; 4 – microcrystalline aggregates; 5 – orthorhombic prismatic microcrystals inside 'empty crystallites' nuclei, the source of (2).

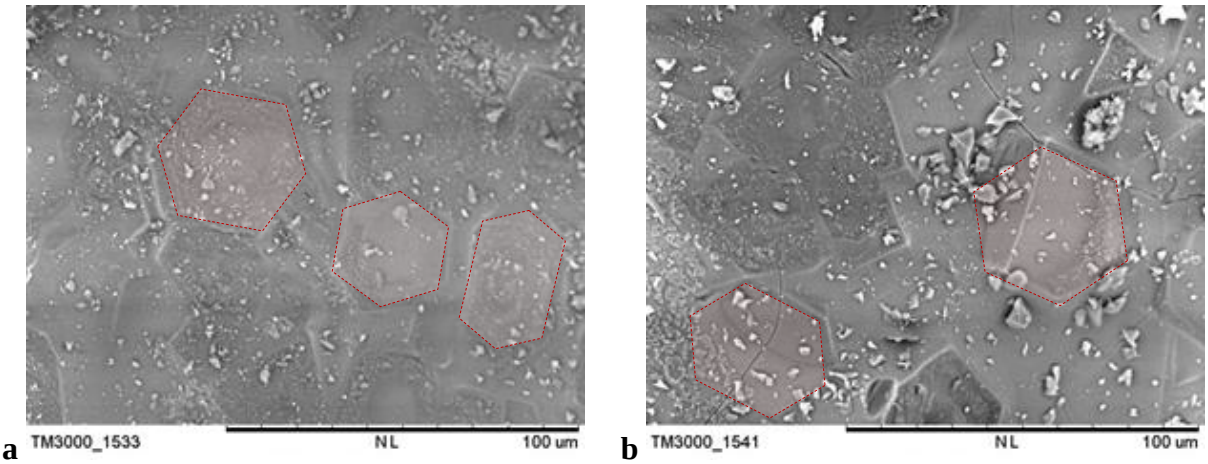

Fig. 3.7. Wall surface of untreated samples A5 1300 (a) and N5 1300 (b), 1000× magnification. Some deformed semi-hexagonal crystal areas (α-cordierite) marked with red lines.

The porosity and apparent density data of the samples obtained by the Archimedes method are shown in Fig. 3.8. The samples have a high proportion of total pore volume, generally in the range of 50–75 %. It can be assumed that the values of the apparent porosity of the samples strongly depend on the maximum firing temperature, moreover, it can be clearly seen that the process of pore formation is non-linear with respect to the maximum firing

temperature. Typically, increasing the firing temperature increases the apparent porosity of the sample until it reaches a certain maximum value after which a further increase in temperature causes the opposite phenomenon – apparent porosity which slightly but decreases. The maximum apparent porosity of composition A5 (≈73.3 % ± 2.7 %) is achieved by firing the sample at 1300 °C, but of composition N5 (≈72.1 % ± 4.0 %) – by firing at 1325 °C. All samples have a bulk density in the range of 1.1 g/cm^3 to 1.3 g/cm^3, which makes them only slightly denser than water. Comparing the change in the bulk density of the samples with increasing firing temperature, it can be seen that the samples gradually become less dense, which is inversely comparable to the change in apparent porosity with increasing firing temperature. Although the bulk density values of the A5 samples are generally higher than those of the N5 samples, the lowest bulk density value (1.11 g/cm^3 ± 0.01 g/cm^3) is achieved for the A5 sample, which, in inverse proportionality to the apparent porosity data, decreases rapidly by firing at 1300 °C. Similarly, samples of composition N5 show a steady decrease in bulk density when firing temperature is increased, reaching its lowest value (1.13 g/cm^3 ± 0.02 g/cm^3) at 1325 °C. Control sample's K0 porosity is very small – only 1.3 % and bulk density – 2.3 g/cm^3.

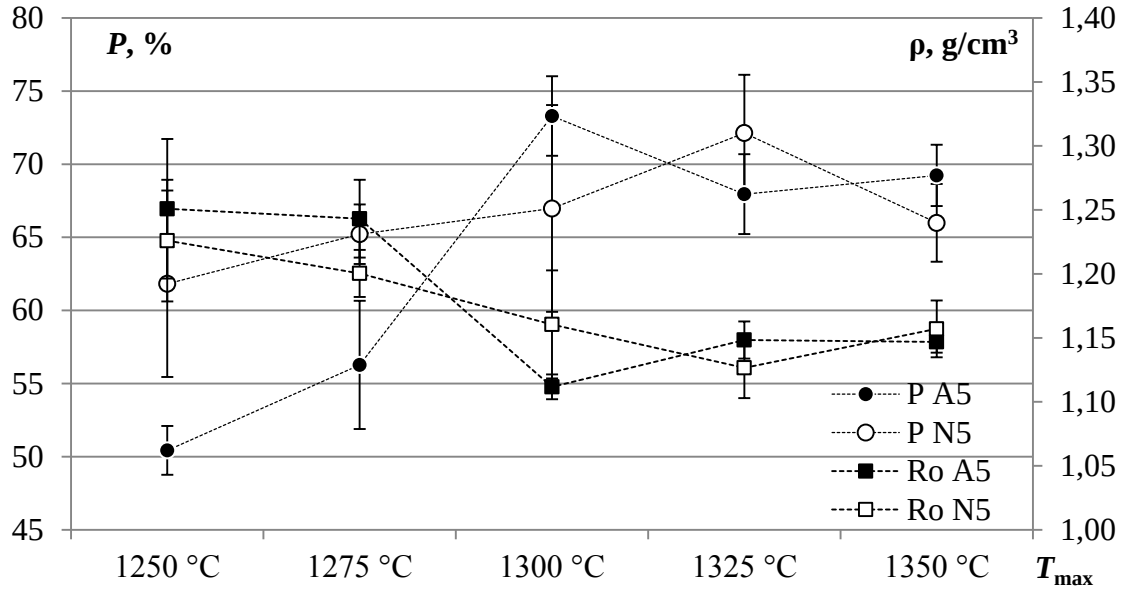

Fig. 3.8. Porosity (*P*) and bulk density (ρ) of samples A5 (●, ■) and N5 (○, □) dependent on maximum firing temperature (T_{max}).

Mercury intrusion porosimetry provides data on pores in a material in a limited range that practically does not exceed 0.006–1000 μm. From the results of surface microscopy, it can be seen that most of the pores forming the macroscopic pore structure of all samples are larger than 0.5 mm, thus it can be concluded that the information provided by mercury porosimetry refers mainly to pores in the pore walls of the samples. These micro-sized pores (in this context, pores with a diameter between 0.1 μm and 1000 μm) make up only a small part of the total sample volume. However, the presence, size and amount of microscopic pores in the sample also play an important role, as the presence of such structural elements increases the ability of the material to attract various chemically active compounds, including micro- and

nano-sized particulate catalysts, surfactants, etc. Table 3.3 summarizes the mercury porosimetry data of the samples, and, as the results show, the evolution of the micropore formation of the samples depending on the firing temperature is specific and differs significantly between the compositions.

Table 3.3

Mercury Intrusion Porosimetry for Samples Obtained at 1250 °C, 1300 °C and 1350 °C

Sample	**Distribution**	**Pore size range**	**Pore vol., cm^3/g**	**Porosity, %**
A5 1250	bimodal	>75 % 30–60 μm; <25 % 100–200 μm	0.30	6.00
A51300	monomodal	>80 % 100–200 μm	0.42	9.30
A51350	bimodal	>75 % 1–2 μm; <25 % 100–200 μm	1.60	25.79
N51250	polymodal	>50 % 100–200 μm	0.03	0.51
N51300	monomodal	>90 % 0.1–0.2 μm	3.00	45.38
N51350	monomodal	>90 % 70–200 μm	0.43	8.39

For example, the size distribution of microscopic pores (Fig. 3.9) of sample A5 at 1250 °C is bimodal; more than 75 % of these pores are in the size range of 30–60 μm, but less than 25 % – in the size range of 100–200 μm. However, the proportion of micropores in the material is relatively small, less than 0.3 cm^3/g, but the porosity caused by the pores of this range is 6.00 % (the total porosity of the sample of this composition is >50 %).

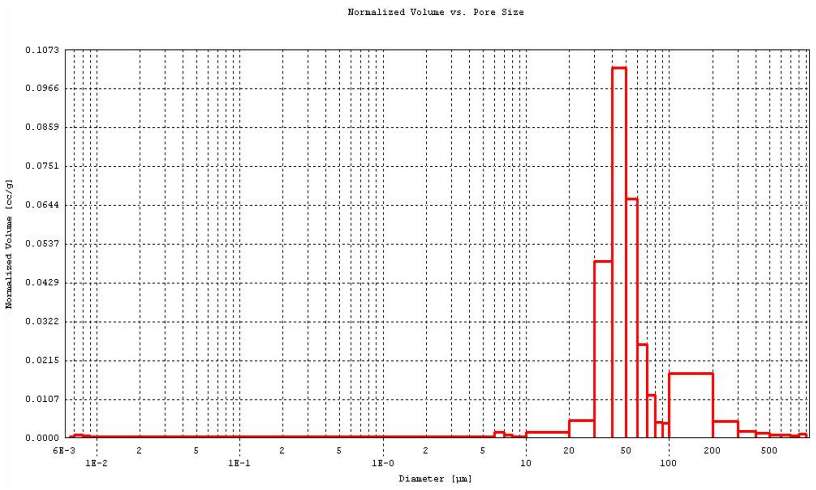

Fig 3.9. Mercury intrusion data for pore size distribution of sample A5 1250 (in μm).

When firing temperature is increased to 1300 °C, an increase in micropore size and proportion as well as a monomodal pore size distribution formation is observed in the sample. In this sample, more than 80 % of all micropores are in the size range of 100–200 μm, with the remainder being slightly below or above this range. The proportion of pores of this size

range has increased to 0.42 cm^3/g, and prosity – to 9.3 %. By raising the firing temperature to 1350 °C, the formation of micropores of the bimodal distribution is observed in the sample, and most of the pores are much smaller than before, in the range of 1–5 μm, and only ≈25 % of the pores are 100–200 μm in size. As the total porosity of this sample decreased compared to the sample obtained at 1300 °C, the natural result would be a decrease of the microporous porosity, but, contrary to expectations, the microporous porosity turned out to increase to 25.79 % and the pore volume to 1.6 cm^3/g.

In contrast, for the sample of composition N5 obtained at 1300 °C, the micropore distribution is scattered in wide range; more than 50 % of the pores are in the size range of 100–200 μm, while the remainder is divided into approximately equal parts between 10–100 μm and 200–900 μm. In addition, the volume and porosity of this sample is particularly low.

Raising the firing temperature to 1300 °C (Fig. 3.10) gives a sample in which the micropore distribution is very different from the sample obtained at a lower temperature: the micropore distribution is very narrow and more than 90 % of these pores are between 0.1 μm and 0.2 μm but less than 5 % in the range of 40 μm to 300 μm. In particular, the volume fraction of these smaller micropores is unexpectedly high – about 3.0 cm^3/g, and the porosity produced by these pores is about 45.38 %.

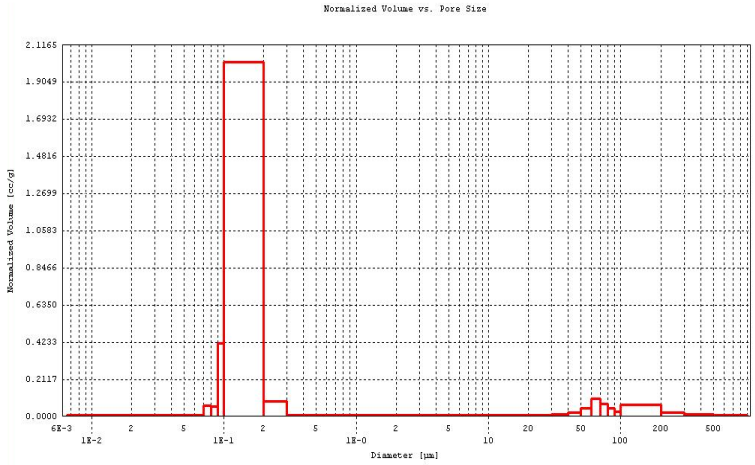

Fig. 3.10. Mercury intrusion data for pore size distribution of sample N5 1300 (in μm).

By raising the firing temperature to 1350 °C, the N5 samples repeatedly change their pore distribution, apparently mimicking the 1250 °C pore distribution. The only difference is that the pore distribution has become slightly narrower – more than 50 % of the pores are in the range of 80–200 μm and with a higher proportion – 0.43 cm^3/g. The porosity formed by these pores is 8.39 %. Therefore, it must be concluded that a continuous increase in the firing temperature is not clearly favourable for the formation of micropores. Depending on the composition there is a definite, experimentally determinable, narrow firing temperature range, below or above which competing macropore formation process is favoured. The optimal firing temperature of the compositions studied in the work, from the point of view of micropore formation, is about 1300 °C.

3.3. Mechanical Properties

Compressive (σ_c) and flexural (σ_f) strength of samples from A5 and N5 compositions depending on the firing temperature are given in Fig. 3.11. Samples of both compositions are characterized by a decrease in compressive and flexural strength with increasing firing temperature. Samples from the N5 composition show higher strength values, which is interesting considering that the samples of this composition have higher pore content than the A5 samples. Thus, possible differences result in microstructural differences in the solid phase composition of the two materials. It should be remembered that the N5 samples of the composition are characterized by smaller pore size and larger pore surface area, which thus proves the existence of a finer structure. The pore walls of such a structure have a higher total mechanical strength compared to the A5 samples of the respective temperature composition whose pores are on average larger, and, consequently, the pore wall structure is less mechanically strong.

The samples of both compositions reach their maximum values at 1275 °C, followed by a gradual decrease in the strength value and reaching a minimum already at 1325 °C for composition A5 and 1350 °C for composition N5. The decrease in strength corresponds to an increase in porosity, yet no sudden decrease in strength was observed for sample A5 obtained at 1300 °C, although a rapid increase in porosity was previously observed at this temperature.

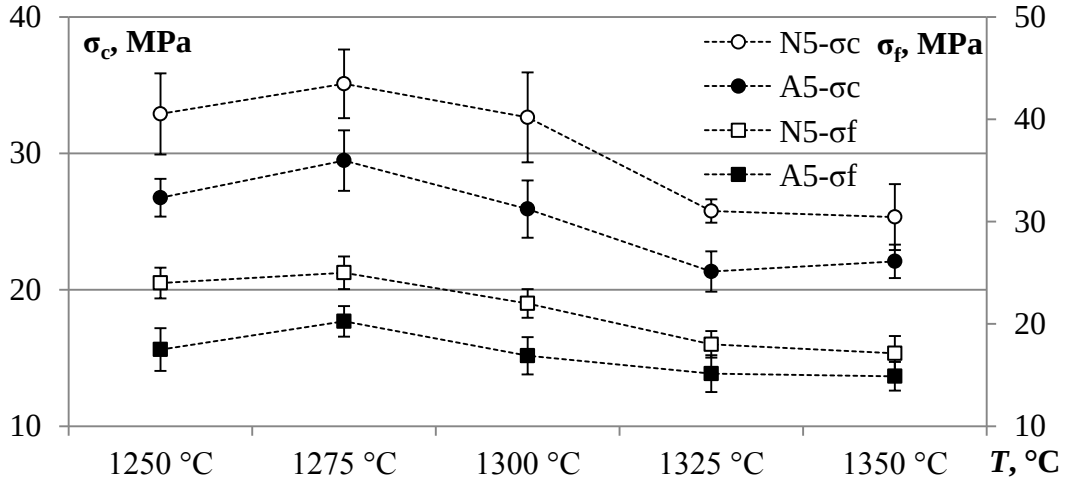

Fig. 3.11. Compressive (σ_c) and flexural (σ_f) strength of samples A5 (●, ■) and N5 (○, □) depending on firing temperature (*T*).

In general, the strength values of both compositions are satisfactory, considering that both compositions have compressive strength values above 20 MPa for all firing temperatures, despite the relatively high pore content. A strong correlation was found between the compressive and flexural strengths of the samples of both compositions, e.g., the Pearson correlation coefficients of these values are calculated as $r_{N5} = 0.982$ and $r_{A5} = 0.995$, which indicates a strong positive correlation. Accordingly, the coefficients of determination $r_{N5}^2 = 0.964$ and $r_{A5}^2 = 0.990$ indicate that the compressive and flexural strengths of both compositions are practically affected by the same conditions which are most likely the

porosity and pore distribution of the samples as well as the viscoelastic processes associated with the solid phase composition (crystalline/amorphous phase ratio, grain sizes).

The modulus of elasticity of both compositions was determined by two methods: in the first case – using flexural strength, and in the second – dynamic mechanical analysis (DMA) test data. Both methods use a 3-point bending configuration model, but the DMA test does not destroy the sample, unlike the flexural strength test, which means that DMA is more economical to required amount of test material. The data of the calculated elastic moduli (E_f and E_d) are shown in Fig. 3.12. Moduli values of N5 samples are slightly higher than those of A5. The highest values are achieved by firing the samples at 1275 °C, but the lowest – at 1325 °C, which, within margin of error, is comparable to the values of samples obtained at 1350 °C.

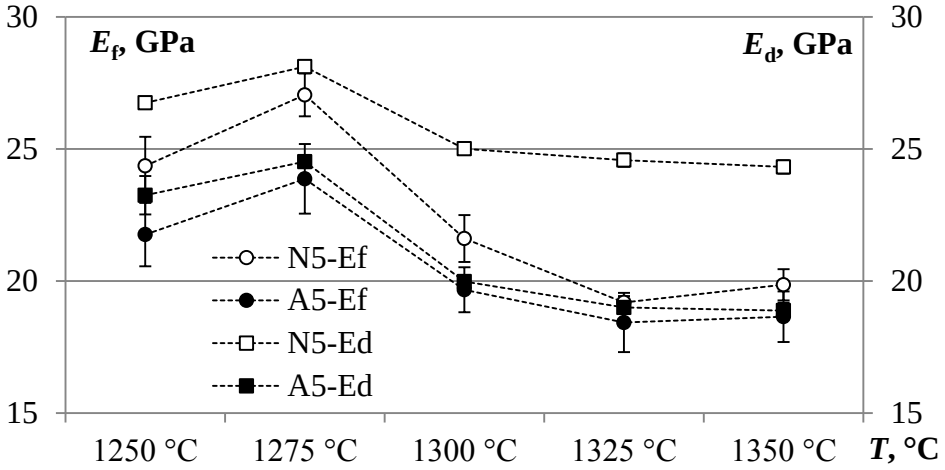

Fig. 3.12. Elastic moduli of samples A5 (●, ■) and N5 (○, □) depending on firing temperature (T). Results obtained from the data of flexural (E_f) and DMA (E_d) method.

Both methods are equally suitable for determining the modulus of elasticity of porous ceramic samples: linear regression analysis shows that the data provided by both methods have a very high degree of positive correlation (Pearson correlation coefficients for N5 and A5 are $r_{N5} = 0.984$ and $r_{A5} = 0.986$, respectively).

3.4. Thermal properties

Probably the most important thermal property of cordierite ceramics is the characteristically low CTE, typically not exceeding $4.0 \cdot 10^{-6}$ °C^{-1}. The mean CTE values obtained by dilatometry for samples A5 and N5 are summarized in Table 3.4.

Table 3.4

Average CTE Values of Samples A5 and N5, α_{avg}, °C^{-1} (100–1000 °C)

Sample	1250 °C	1275 °C	1300 °C	1325 °C	1350 °C
A5	$3.05 \cdot 10^{-6}$	$2.92 \cdot 10^{-6}$	$2.98 \cdot 10^{-6}$	$2.90 \cdot 10^{-6}$	$2.61 \cdot 10^{-6}$
N5	$2.82 \cdot 10^{-6}$	$2.73 \cdot 10^{-6}$	$2.73 \cdot 10^{-6}$	$2.72 \cdot 10^{-6}$	$2.63 \cdot 10^{-6}$

The CTE values of all composition A5 samples gradually increase with increasing temperature, reaching a partial glass transition in the range of 720–800 °C, which is typical for cordierite crystalline phase based glass-ceramic materials [29]. The differences between the samples obtained at different temperatures are small, about $\pm 0.5 \cdot 10^{-6}$ °C^{-1}. It is also similar for N5 samples: glass transition occurs in the 720–800 °C range, which indicates that both A5 and N5 samples have significant glassy phase content. The CTE of individual N5 samples, depending on the firing temperature, are also small, not exceeding $0.2 \cdot 10^{-6}$ °C^{-1}. Comparing the samples of A5 and N5 compositions, certain differences are observed: the CTE of the composition A5 samples are higher than the corresponding N5 samples at the same firing temperature, moreover, the CTE values within A5 samples have a larger deviation. For sample A5 obtained at 1350 °C, an apparent double glass transition point was observed at around 780 °C and 900 °C. It was also observed that the decrease in CTE for the A5 samples after glass transition point is less rapid, with a tendency to form a plateau. Comparing the sample CTE with each other, it can be seen that the lowest values are for the samples obtained at 1350 °C, but the highest – for the samples obtained at 1250 °C.

For the samples of compositions A5 and N5 (1300 °C), as well as for the sample of base composition K0, extra thermal properties were determined by means of laser 'flash' analysis. In total, three parameters were determined, viz. thermal diffusion (a), thermal conductivity (λ) and specific heat (c_p); the λ values of the samples depending on the ambient temperature are shown in Fig. 3.13. Thermal conductivity coefficient for samples A5 and N5 are evaluated as acceptable. For comparison, the thermal diffusion of 10–24 % porous cordierite samples at room temperature is 1.1–1.4 mm^2/s, which gives, respectively, thermal conductivity coefficients in the range of 1.5–2.5 W/(m·K) [30]; in turn, the thermal diffusion of the samples obtained in this work at room temperature is ≤0.8 mm^2/s at a total porosity of 67–73 %, and the corresponding thermal conductivity coefficients are in the range of 0.55–0.67 W/(m·K).

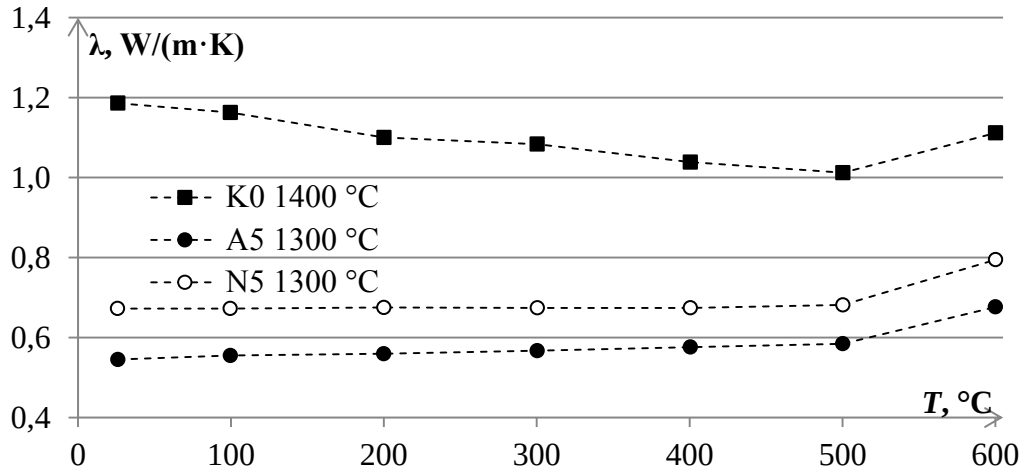

Fig 3.13. Thermal conductivity coefficients of samples K0, A5 1300 °C and N5 1300 °C (λ) depending on ambient temperature (T).

Interestingly, the λ value of the base sample (K0) decreases with increasing ambient temperature, but for samples A5 and N5 it increases very slowly; this tendency is observed up to 500 °C; after this temperature a rapid increase of this value was observed in all samples.

Samples obtained at 1300 °C were also intensively tested to determine materials' resistance to cyclic thermal shock. The results of these tests are shown in Fig. 3.14 which shows the change of the modulus of elasticity of the samples after each repeated thermal shock cycles. The initial modulus of elasticity of the samples of both compositions is similar. It should be noted that the values of the modulus of elasticity determined by the acoustic method are slightly different from the values obtained by the flexural tests, which can be explained both by differences in sample dimensions and test method which is based on sound propagation speed analysis within samples, but in the flexural test – on the principles of a modified Hooke's law. After each thermal shock cycle, the values of the modulus of elasticity of the samples decrease, rapidly in the initial cycles but to a lesser extent in the subsequent cycles. The reason for the decrease in the modulus of elasticity is mainly due to the progressive formation and accumulation of microcracks and defects in the material as a result thermoelastic stresses caused by thermal shock. As a result of the formation of microcracks and pores, the overall integrity of the samples decreases, the material becomes less flexible and is subject to potential catastrophic collapse. According to ASTM C1525, the empirically determined catastrophic collapse limit of a sample is more than a 30 % reduction from the original modulus of elasticity (gray dashed line in the figure). A total of 10 thermal shock cycles were performed on the samples; sample A5 1300 °C passed all 10 test cycles without reaching the elastic modulus reduction threshold of more than 30 %, while sample N5 1300 °C reached this limit twice – after cycles 5 and 10. It can be concluded that the materials made of composition A5 are more resistant to thermal shock than composition N5.

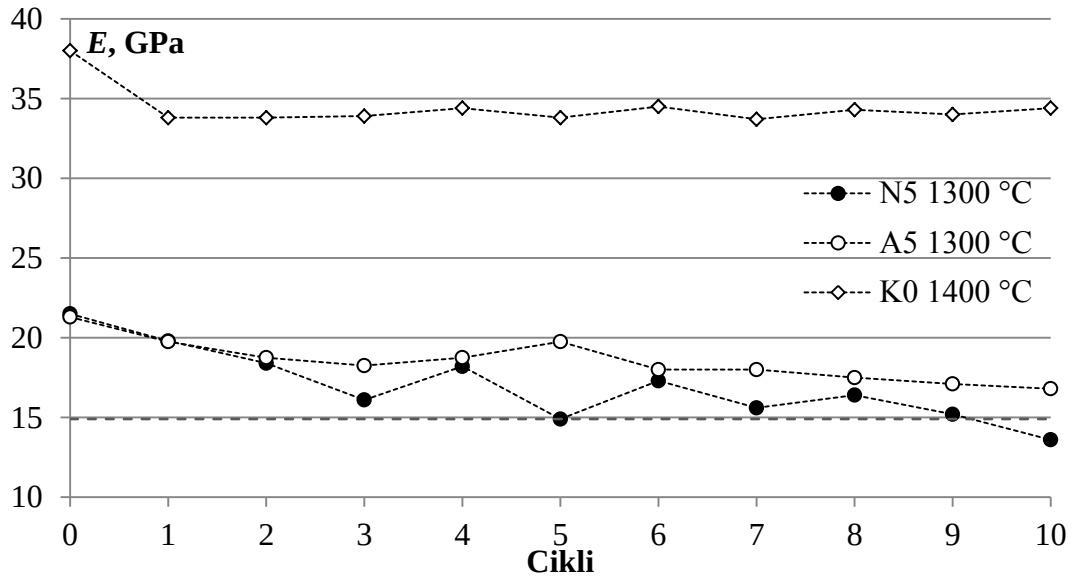

Fig. 3.14. Change of elastic moduli of samples A5 1300 °C and N5 1300 °C as a result of cyclic thermal shock.

The tests revealed a phenomenon that could be described as a ‘self-healing effect’. This effect manifests itself in an unexpected increase in the modulus of elasticity of the material after a discrete number of thermal shock cycles, which occurs markedly once for sample A5 after thermal shock cycle 3 and thrice for sample N5 after thermal shock cycles 3, 5 and 7. The reason for the effect is most likely to be found in the thermal shock test methodology – the samples are reheated at a relatively slow rate of temperature rise and maintained at a maximum temperature for 30 minutes to achieve a homogeneous temperature distribution. As a result, the material acquires additional energy which, in the author’s opinion, is used to:

- promote grain growth in the material, or
- create additional liquid/glassy phase which fills the structural defects formed in the previous cycle, thus acting as a structure-binding agent.

CONCLUSIONS

1. In this work the development process of pore-containing cordierite ceramics has been studied using lightly melting two types of illite clays as pore formers. Samples with a clay additive synthesized at temperatures of 1250 °C and higher have shown to form micro- and macro-sized pores, reaching an apparent porosity of ≈70 % at a firing temperature of about 1300 °C.
2. It is shown that mechanism of pore formation is a physico-chemical process that develops gradually during the sample firing process and can be described as follows: at temperatures above 1100 °C a highly viscous liquid phase forms that begins to 'boil' around 1250 °C and forms gaseous bubbles in the sample mass, the primary source of which is oxygen formed as a result of iron oxide transition reaction. The porosity of the samples increases with the maximum temperature to a critical point after which the viscosity of the liquid phase becomes low enough for the gas bubbles to be effectively released.
3. As a result of the research, it was found that the temperature of α-cordierite formation for the compositions described in this work is approximately 1310 °C. A wide temperature range of melting between 1100 °C and 1300 °C are observed for the compositions.
4. X-ray diffraction analysis indicates that the obtained samples are dominated by cordierite in the crystalline phase, the proportion of which is more than 90 %. The main secondary phase formed in the samples is magnesium spinel. A mixture of α/β cordierite is formed in the samples rather than their separate polymorph phases.
5. It was determined that a complex three-phase (crystalline, amorphous and porous) microstructure is formed in the samples, which is indicated by the visible formation of hexagonal forms even at the macroscopic level, the amorphous phase separating it from fine orthorhombic-shaped crystallite aggregates. Areas of hexagonal shape are the growing phase of α-cordierite which develops by the mechanism of a hopper crystal. At their centre is a fine-crystalline phase of β-cordierite which is connected to the phase of α-cordierite by a vitreous transition phase.
6. The samples contain two types of macropores, 0.2 mm to 0.8 mm in diameter and 10 μm to 20 μm in diameter. The first type of macropores is formed mainly as a result of the mechanism of iron oxide transition reactions and forms the main part of the material pore structure but the second type – as a result of defects and internal stresses in the material wall structure.
7. Thermal conductivity of the samples is low; for porous ceramic samples with clay raw material it [0.6 W/(m·K)] is about twice less than for the base composition cordierite ceramic sample [1.2 W/(m·K)].
8. Porous ceramic samples obtained at 1275 °C show relatively high compressive (≈29–35 MPa) and bending (≈20–25 MPa) strength values which indicate the mechanical stability of the material and open the possibility for its wider practical use.

9. The thermal shock resistance of the samples has been determined by correlating it with the changes in the modulus of elasticity after repeated exposure of the samples to rapid temperature changes from 950 °C to 20 °C. The largest decrease in the modulus of elasticity in all samples is observed after the first thermal shock cycle, but repeated thermal shock cycles have flatter changes in value. Samples of composition A5 withstand all thermal shock cycles, while the sample of composition N5 reaches the critical limit twice, after the 5th and 10th thermal shock cycles.
10. During thermal shock cycles, the samples show a 'self-healing' effect, as a result of which the modulus of elasticity increases after the decrease of the modulus of elasticity caused by the primary thermal shock cycle. Two assumptions can be put forward to explain this effect:
    - grain growth occurs in the material due to the additional energy input during the thermal shock test preparation process, or,
    - during the thermal shock cycles, an additional liquid phase is formed which fills in the structural defects formed in the previous cycle, acting as a cementing agent.
11. The developed material obtaining technology is suitable for the production of porous cordierite ceramics which could be used as a catalyst support in various liquid/gas filtration and purification processes from organic pollutants.

REFERENCES

[1] Janković-Častvan I, Lazarević S, Jordović B, et al. Electrical properties of cordierite obtained by non-hydrolytic sol-gel method. *J Eur Ceram Soc* 2007; 27: 3659–3661.

[2] Goren R, Ozgur C, Gocmez H. The preparation of cordierite from talc, fly ash, fused silica and alumina mixtures. *Ceram Int* 2006; 32: 53–56.

[3] Šperberga, I., Sedmalis, U., Sedmale, G. *Silikātu un grūti kūstošu nemetālisku materiālu fizikālā ķīmija*. Rīga: Rīgas Tehniskā Universitāte, 2010.

[4] Fuji M, Shiroki Y, Menchavez RL, et al. Fabrication of cordierite filter by in-situ solidification for high temperature dust collection. *Powder Technol* 2007; 172: 57–62.

[5] Reda AE, Ahmed SE, Aziz DAA, et al. Sintering and dielectric behavior for doped cordierite by xCuO within MgO(1-x)–Al2O3–SiO2 ceramics. *Mater Chem Phys* 2020; 243: 122616.

[6] Benito JM, Turrillas X, Cuello GJ, et al. Cordierite synthesis. A time-resolved neutron diffraction study. *J Eur Ceram Soc* 2012; 32: 371–379.

[7] Karkhanavala MD, Hummel FA. The Polymorphism of Cordierite. *J Am Ceram Soc* 1953; 36: 389–392.

[8] Obradović N, Dordević N, Filipović S, et al. Influence of mechanochemical activation on the sintering of cordierite ceramics in the presence of Bi2O3 as a functional additive. *Powder Technol* 2012; 218: 157–161.

[9] Janković-Častvan I, Lazarević S, Tanasković D, et al. Phase transformation in cordierite gel synthesized by non-hydrolytic sol-gel route. *Ceram Int* 2007; 33: 1263–1268.

[10] Miyashiro A, Iiyama T, Miyashiro T, et al. The polymorphism of cordierite and indialite. *Am J Sci* 1955; 253: 185–208.

[11] Gibbs G V. The polymorphism of cordierite. I. The crystal structure of low cordierite. *Am Miner* 1966; 51: 1068–1087.

[12] Meagher EP, Gibbs G V. The polymorphism of cordierite. II. The crystal structure of indialite. *Can Miner* 1977; 15: 43–49.

[13] González-Velasco JR, Ferret R, López-Fonseca R, et al. Influence of particle size distribution of precursor oxides on the synthesis of cordierite by solid-state reaction. *Powder Technol* 2005; 153: 34–42.

[14] Acimovic Z, Pavlovic L, Trumbulovic L, et al. Synthesis and characterization of the cordierite ceramics from nonstandard raw materials for application in foundry. *Mater Lett* 2003; 57: 2651–2656.

[15] Zhou JE, Dong Y, Hampshire S, et al. Utilization of sepiolite in the synthesis of porous cordierite ceramics. *Appl Clay Sci* 2011; 52: 328–332.

[16] Bejjaoui R, Benhammou A, Nibou L, et al. Synthesis and characterization of cordierite ceramic from Moroccan stevensite and andalusite. *Appl Clay Sci* 2010; 49: 336–340.

[17] Ghitulica C, Andronescu E, Nicola O, et al. Preparation and characterization of cordierite powders. *J Eur Ceram Soc* 2007; 27: 711–713.

[18] Chotard T, Soro J, Lemercier H, et al. High temperature characterisation of cordierite-mullite refractory by ultrasonic means. *J Eur Ceram Soc* 2008; 28: 2129–2135.

[19] Costa Oliveira FA, Cruz Fernandes J. Mechanical and thermal behaviour of cordierite-zirconia composites. *Ceram Int* 2002; 28: 79–91.
[20] Camerucci MA, Urretavizcaya G, Castro MS, et al. Electrical properties and thermal expansion of cordierite and cordierite-mullite materials. *J Eur Ceram Soc* 2001; 21: 2917–2923.
[21] Ranachowski J, Ranachowski P, Ciesla M, et al. Modern arc-resistant materials for welding technology. *Ind Ceram* 1999; 19: 103–106.
[22] Dimitrijevic M, Posarac M, Majstorovic J, et al. Behavior of silicon carbide/cordierite composite material after cyclic thermal shock. *Ceram Int* 2009; 35: 1077–1081.
[23] Zhiming S. Preparation of Cordierite Ceramic Using Mixtures of Ce4+ -Modified Amorphous Powder and Oxide Powders. *J Rare Earths* 2006; 24: 263–265.
[24] Gass SE, Sandoval ML, Talou MH, et al. High Temperature Mechanical Behavior of Porous Cordierite-based Ceramic Materials Evaluated Using 3-point Bending. *Procedia Mater Sci* 2015; 9: 254–261.
[25] Yamuna A, Johnson R, Mahajan YR, et al. Kaolin-based cordierite for pollution control. *J Eur Ceram Soc* 2004; 24: 65–73.
[26] Chen G. Sintering, crystallization, and properties of CaO doped cordierite-based glass-ceramics. *J Alloys Compd* 2008; 455: 298–302.
[27] Stinkule, A., Stinkuls, Ģ. *Latvijas derīgie izrakteņi*. Riga: University of Latvia, 2013.
[28] Mercury JMR, Pena P, De Aza AH, et al. On the decomposition of synthetic gibbsite studied by neutron thermodiffractometry. *J Am Ceram Soc* 2006; 89: 3728–3733.
[29] Todhunter R. *Crystalline phase development in cordierite glass-ceramics*. University of Warwick, 1984.
[30] García E, Osendi MI, Miranzo P. Thermal diffusivity of porous cordierite ceramic burners. *J Appl Phys* 2002; 92: 2346–2349.